Surface & Coatings Technology 203 (2009) 3325–3331

Contents lists available at ScienceDirect

Surface & Coatings Technology

journal homepage: www.elsevier.com/locate/surfcoat

Mechanical characterization of nano-reinforced silica based sol–gel hybrid coatings on AISI 316L stainless steel using nanoindentation techniques

Josefina Ballarre [a,*], Emilio Jimenez-Pique [b], Marc Anglada [b], Sergio A. Pellice [a], Ana L. Cavalieri [a]

[a] Material's Science and Technology Research Institute (INTEMA), UNMdP-CONICET Juan B. Justo 4302, B7608FDQ, Mar del Plata, Argentina
[b] Departament de Ciència dels Materials i Enginyeria Metallúrgica, Universitat Politècnica de Catalunya, Avda. Diagonal, 647 (ETSEIB), 08028 Barcelona, Spain

ARTICLE INFO

Article history:
Received 3 February 2009
Accepted in revised form 14 April 2009
Available online 20 April 2009

Keywords:
Silica coatings
Nanoindentation
Mechanical properties
Orthopaedic stainless steel

ABSTRACT

One way to enhance the surface properties of metals used as surgical implants such as wear or protective behaviour is to use hybrid organic–inorganic sol–gel coatings. The addition of SiO_2 colloidal particles to some hybrid formulation is thought to give films with bigger thickness than the coatings without particles, acting as mechanical reinforcement and to make an adequate surface to resist the extreme surgical procedures taking place in orthopaedic replacements.

Coatings made by sol–gel with tetraethoxysilane (TEOS) and methyltriethoxysilane (MTES) with the addition of silica nanoparticles were applied onto surgical grade stainless steel. One of the most recent techniques used to study the mechanical properties of thin films is the instrumented indentation, known as nanoindentation, was used to evaluate elastic modulus, hardness and friction coefficient. This is a superficial technique used to measure quasi-statically the penetration of an indenter at increasing loads applied to very little volumes of material.

The mechanical properties values found for the TEOS–MTES–10%SiO_2 coating are smaller than for the 30% filled coating, and higher that the coating without nanoparticles. In the scratch test of the TEOS–MTES–SiO_2 30 wt.% coating it can be seen that in this case the failure takes place at higher applied load than for the less silica reinforced one, indicating a much better adhesion than the system with 10% of SiO_2 nanoparticles.

1. Introduction

Bio-inert materials are commonly used in medicine; however not all the materials can be used for orthopaedic purposes. Because of the high mechanical properties required for orthopaedics metals are the most widely used materials [1]. However, they are not able to create a natural union with the mineralized bone, and these prosthetic materials could also release metallic particles to the surrounding media, causing different pathologies that could finally lead to the removal of the implant [2,3]. One way to improve metallic implant performance is by the application of protective films [4,5]. Some of these coatings are mainly made from alcoxide precursors of SiO_2 which create vitreous and uniform films. The films can be functionalized introducing particles in the system, or can be bioactive themselves [6–10].

A disadvantage of glassy coatings is their brittleness. Hybrid organic–inorganic films with high content of silica are an alternative to improve the mechanical properties of vitreous coatings since they preserve the property of being a protective and dense net. In addition, the incorporation of hydroxides with some organic groups is expected to give plastic characteristics to the films.

Thin films provide the material the capability of being a bio-inert connector between the metallic prosthesis and the bone tissue. Also, superficial features as toughness, friction coefficient and adhesion of the coating to the substrate are of great importance for a complete mechanical characterization. The orthopaedic prosthesis is inserted in the human body without paying special attention in the type of material or if it is a coated one, therefore the mechanical, adhesive and wear behaviour of their surfaces is a very important issue. One of the most recent techniques used to study the mechanical properties of thin films is instrumented indentation, also known as nanoindentation when the resolution of the instrument is in the nanometer. In this technique, a load is applied to an indenter and the displacement into the material is recorded simultaneously. Analysis of the load (P)–penetration (h) curves allows for the extraction of mechanical parameters, mainly hardness and Young's modulus without the need of visualizing the imprint.

The present work takes care of the mechanical behaviour of synthesized hybrid organic–inorganic coatings with the addition of silica nanoparticles. The nanoparticles are use with the aim of slightly increase the protective coating thickness. Certainly, this increase is wanted meanwhile does not affect the implant geometry. These coatings are thought to be used as coatings for orthopaedic implants with three objectives: be a protective layer to the wear and frictional events, to avoid or prevent the release of ions or metallic particles due to corrosion, and to be a useful support for adding bioactive particles

* Corresponding author. Tel.: +54 223 481 6600; fax: +54 223 4810046.
E-mail address: jballarre@fi.mdp.edu.ar (J. Ballarre).

0257-8972/$ – see front matter © 2009 Elsevier B.V. All rights reserved.
doi:10.1016/j.surfcoat.2009.04.014

to the surface to generate bioactivity and a natural union between the metallic implant and the existing bone. In previous works the corrosive and bioactive behaviour of similar hybrid sol–gel coatings were analyzed [11–15], and it is for nearly future work that these properties are going to be evaluated for the TEOS–MTES–SiO_2 coatings.

Some mechanical properties of TEOS–MTES and similar hybrid coatings without the adding of SiO_2 nanoparticles have been previously analyzed [16–18], however there is still a knowledge gap regarding the behaviour of nano-particle reinforced sol–gel coatings. With a lateral force modulus, and a ramped load in a displacement (scratch) path, a nano-scratching test can be done on the coated sample surface [19–22]. The objective of this work is to advance in the understanding of the elastic-plastic, frictional and adhesive behaviour of organic–inorganic hybrid silica based coatings reinforced with SiO_2 nanoparticles and deposited on stainless steel, by the application of nanoindentation techniques.

2. Experimental procedure

2.1. Preparation of the sols

Hybrid organic–inorganic sols were prepared with a silicon alkoxide, tetraethylorthosilicate (TEOS, 99% ABCR), an alkylalkoxide, methyltriethoxysilane (MTES, 98% ABCR) and a water based solution with colloidal silica (LEVASIL 200A 40 wt.%, Bayer). The molar ratio of the alcoxides always remained constant (TEOS/MTES = 40/60) while the addition of colloidal silica was the variant: 10 or 30 mol%. The final silica concentration for both sols was 4.16 mol/L. The amount of water was kept stoichiometric.

2.2. Substrates and coatings

Coatings were deposited on stainless steel AISI 316L (Atlantic Stainless Co. Inc., composition: C 0.03% max, Mn 2% max, Si 1% max, P 0.045% max, S 0.03% max, Ni 10–14%, Cr 16–18%, Mo 2–3%). Sheets of 2×2 cm^2 were used as substrates. They were degreased, hand washed with distilled water, and rinsed in ethanol previous to the deposition of the films.

A first layer prepared with TEOS–MTES–SiO_2 sol was obtained at room temperature by dip-coating at a withdrawal rate of 25 cm min^{-1} or 18 cm min^{-1} for 10% and 30% of colloidal silica respectively. Afterwards, the sample was dried at room temperature for 30 min, and heat treated for 30 min at 450 °C in an electric furnace. A second layer was made by applying TEOS–MTES–SiO_2 10% on the top of the first one (either with 10 or 30% in weight of SiO_2 nanoparticles). The withdrawal and thermal treatment was the same used for the first layer in the same conditions.

Coating homogeneity and appearance was evaluated by scanning electron microscopy (HITACHI S-4700 field emission). Coating thickness was measured for each layer on glass substrates after densification by using a profilometer (Talystep, Taylor-Hobson, UK) on a scratch made after deposition.

2.3. Mechanical characterization

The mechanical elastic-plastic properties of the silica-based films were studied using the nanoindentation technique. Both Young's modulus and hardness were determined and other relevant data of the films were analyzed from the load–displacement curves [23]. A Nanoindenter XP (MTS Nano Instruments) with a continuous stiffness module (CSM), was used, allowing the continuous measurement of contact stiffness (S) and load (P) as a function of the penetration depth (h). The indentations were made to a maximum depth of 2000 nm (to a maximum load of about 160 mN), and under a constant deformation rate of 0.05 s^{-1} and 0.5 s^{-1} for the all measurements. A Poision ratio of 0.18 was assumed for the coatings. A three-side pyramid Berkovich indenter was used and it was calibrated against fused silica standard. Multiple indentations (a matrix of 3×3) separated by 100 μm were made in each sample in order to obtain average values.

The results were analyzed by the Oliver and Pharr method [23].

Elastic Modulus is calculated based in the relationships developed by Sneddon [24] and modified by other authors [25,26]. The results were analyzed according to the equation:

$$E_r = \frac{1}{\beta}\frac{\sqrt{\pi}}{2}\frac{S}{\sqrt{A(h_c)}}, \quad (1)$$

where β equal to 1.034 for a Berkovich indenter [27].

During the indentation of coatings and thin films, it is possible that the measured mechanical properties are influenced by the substrate, specially the Young's modulus, where it is generally assumed that the response will be a combination of the coating and the substrate for penetration depths below 1/10 of the coating thickness.

In order to extract the values of the coating, a modelling of the combined response is usually performed, either for elastic modulus [28,29], or for hardness [30–32]. These models generally assume isotropic linear behavior of the materials.

The nano-scratch tests were performed using a nano-indenter XP, MTS Nano Instruments (force resolution: 50 nN; displacement resolution: 0.1 nm) equipped with a nano-scratch attachment that allows lateral force measurements. A pyramidal diamond Berkovich indenter was used to scratch each coating/substrate system and a 700 μm scratching track was applied in all tests. The experimental procedure is showed in the Fig. 1. At first (pre-scan step), the tip approaches the surface under default conditions, and then the load is maintained (0.1 mN) through all the scratch distance (100 μm initial + 500 μm straightforward scratch + 100 μm final). An initial surface profile of the samples is made before scratching. In the second step (scratching), the tip starts to scratch at 100 μm from the start of the experiment with a ramped load to the distance of 600 μm, corresponding to an effective scratch distance of 500 μm (final maximum applied load of 500 mN), where the load is removed to the initial one (0.1 mN) and maintained constant for 100 μm more. The surface profile could be sensed by the depth-sensing system. In the third step (post-scan) the test is done as was described in the pre-scan to measure the elastic recovery after scratching.

Lateral (friction) forces are calculated from the deflexion of the loading column. The coefficient of friction (COF) is calculated by

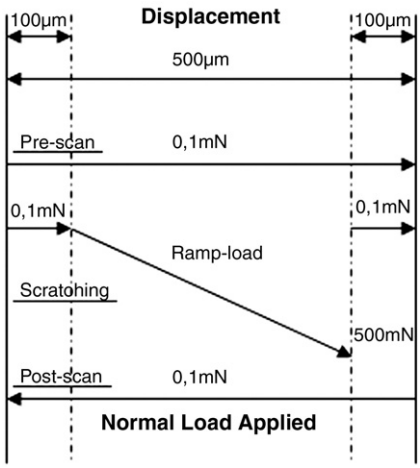

Fig. 1. Schematic diagram of the different steps for the experimental scratch test procedure.

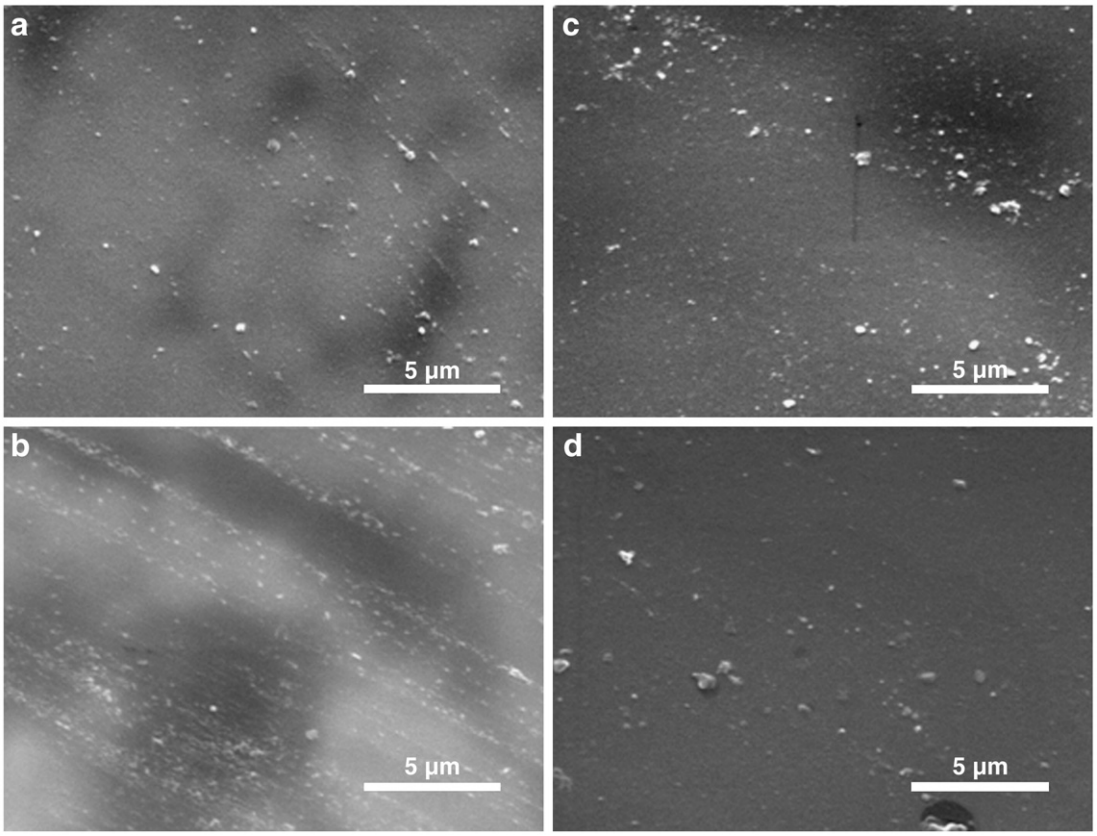

Fig. 2. Scanning Electron Microscopy images of the TEOS–MTES–SiO_2 10 (a and b) and 30 (c and d) wt.% after: 1 (a and c) and 30 (b and d) days of immersion in simulated body fluid.

taking the ratio of the lateral force and the normal load applied on the indenter afterwards [33].

3. Results and discussion

Fig. 2 a and b show the images of TEOS–MTES–SiO_2 coatings with different amount of colloidal particles after 24 h of immersion in simulated body fluid (concentration of inorganic ions similar to body plasma [34], pH 7.25 ± 0.05.), and Fig. 2 c and d show the same kind of coatings after 30 days of immersion. These immersion times were used in order to compare in the near future the SEM micrograph images with other electrochemical methods, such as Potentiodynamic polarization curves and Electrochemical Impedance Spectroscopy (EIS) to analyze the integrity and homogeneity of the coatings, as it was done in previous works [11,13]. Both coatings appear homogeneous and crack-free after immersion, without showing great differences among them. These results are preliminary since other essays with more complex techniques have to be done in order to know better the morphology and structure of the coatings.

The average thickness obtained using the profilometer resulted 2.1 ± 0.2 and 2.3 ± 0.2 μm for the TEOS–MTES–SiO_2 10% and TEOS–MTES–SiO_2 30% single coating, respectively. The coatings containing SiO_2 particles are thicker than the ones without them being the value for the TEOS–MTES coating 1.5 ± 0.2 μm [16]. The nanoparticles of SiO_2 were added to reinforce the films, decreasing the porosity and the conductivity, and filling the defects and holes present in the silica network [35].

In order to compare the indentation data of the two types of coatings, the measurements were carried out at two different deformation rates (0.05 and 0.5 s^{-1}). This change onto the experimental setup parameter of the nanoindentation tests can be noticed in loading–unloading curves of the studied coatings (Fig. 3). The maximum applied load varies in each case since the test is programmed for a given maximum penetration depth. Fig. 3 shows that when the samples are slowly indented or deformed, the maximum applied load is smaller that when a bigger deformation rate is applied. The coatings made with TEOS–MTES and 30 wt.% of silica nanoparticles presented the highest maximum load and it could represent a major stiffness of these kinds of systems. This fact seems to be due to the amount of colloidal spherical nanoparticles, which have a larger elastic modulus than the polymer matrix and could also be compactly packed during nanoindentation process.

Figs. 4 and 5 (a and b) represent the obtained values for the Young's modulus (E) and the hardness (H) versus the penetration depth for the

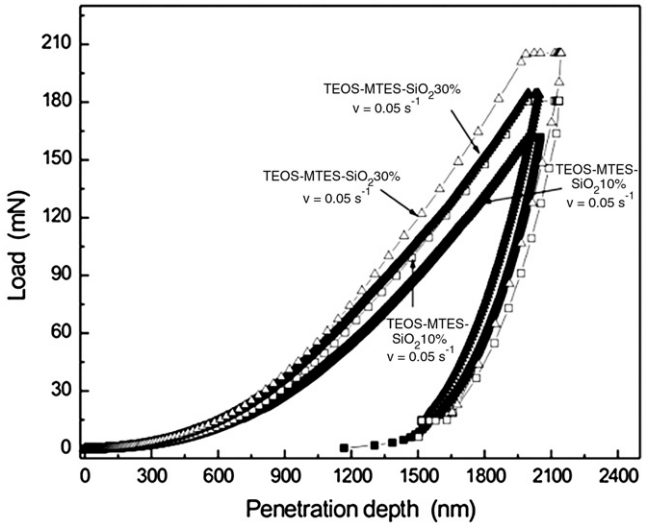

Fig. 3. Load–displacement curves for the TEOS–MTES–SiO_2 coatings with 10% of silica nanoparticles and a deformation rate of 0.05 s^{-1} (■) and 0.5 s^{-1} (□); and for TEOS–MTES–SiO_2 coatings with 30% of SiO_2 and a deformation rate of 0.05 s^{-1} (▲) and 0.5 s^{-1} (Δ).

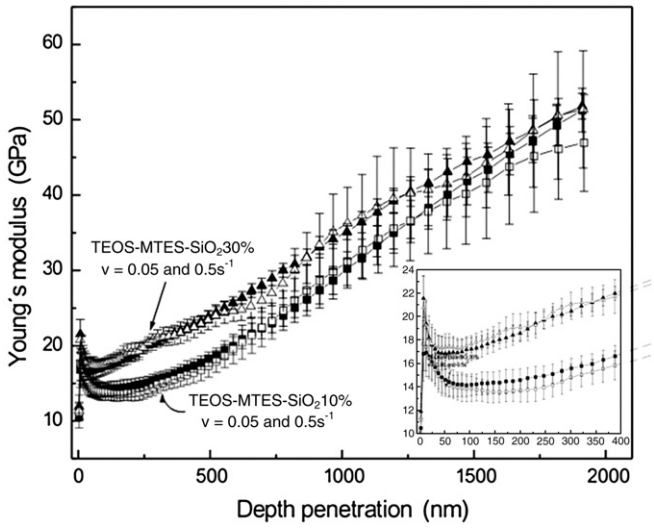

Fig. 4. Young's modulus vs Depth penetration into the coating thickness for the TEOS–MTES–$SiO_2$10% with strain rate of 0.05 s^{-1} (■) and 0.5 s^{-1} (□), and for TEOS–MTES–$SiO_2$30% coating with strain rate 0.05 s^{-1} (▲) and 0.5 s^{-1} (Δ).

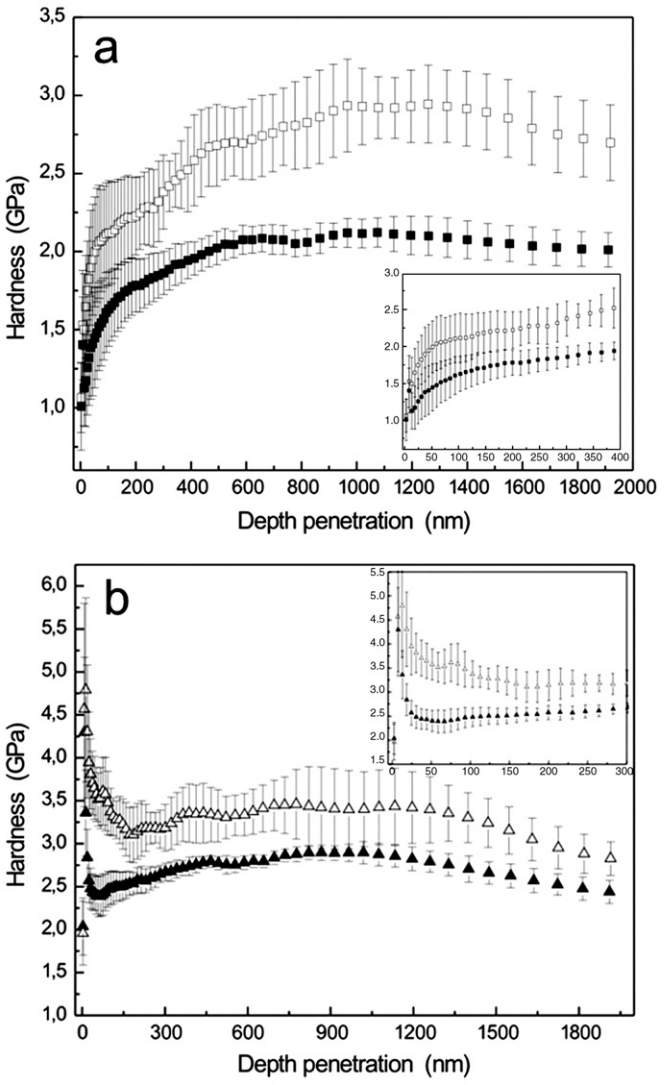

Fig. 5. Hardness vs Depth penetration into the coating thickness for: (a) the TEOS–MTES–$SiO_2$10% with strain rate of 0.05 s^{-1} (■) and 0.5 s^{-1} (□), and for (b) TEOS–MTES–$SiO_2$30% coating with strain rate 0.05 s^{-1} (▲) and 0.5 s^{-1} (Δ).

analyzed samples (with 10 and 30% of colloidal silica nanoparticles), employing the continuous stiffness data. The values of the mechanical properties for the TEOS–MTES coating containing 10 wt.% of silica nanoparticles are smaller than for the 30% filled coating at the first part of the curve, where the influence of the substrate is lower [36]. The main value of the property was taken at 200 nm depth penetration on the coating. Again, this improvement of stiffness is due to an increase of packing events of the nanoparticles in the reinforced coatings. A different effect is noticed in hardness measurements. The samples with major content of silica nanoparticles have again the higher values of H but they seem to be affected by the rate of deformation (Fig. 5 b), showing high values at faster deformation velocities (0.5 s^{-1}) due to visco-elastic effects [37].

The quasi-invariability of the elastic modulus values with the increment of the deformation rate could be explained with the unchanged composition of the TEOS–MTES coating matrix, where the organic and inorganic compounds remained constant. Also other characteristics of the system that could alter the modulus, like temperature and crystallinity ("locked" segments) [35], also remained constant showing almost no change of the Young Modulus with strain rate.

In order to compare the obtained values for the TEOS–MTES–$SiO_2$10 and 30 wt.% coatings, values for hardness and elastic modulus of stainless steel substrate and TEOS–MTES coating are shown in Table 1. The main values were taken at 200 nm depth from the top of the coating and with a deformation rate of 0.05 s^{-1} in order to compare to similar values and avoid visco-elastic effects. Again, it is seen that the addition of SiO_2 nanoparticles increase the Young's modulus and hardness of the coating, also in comparison to the coating without particles studied in previous work [16].

Confocal microscopy images (Fig. 6) were taken after the indentation processes in order to document the indent size and damage around it. Both type of coatings presented the same kind of image: crack propagation after loading–unloading cycle was performed, without knowing the exact moment of the crack formation. Also the generation and propagation of defects are thought to be due by the packing and densification process into the coating (Fig. 6 c).

The Saha and Nix model [28] was used to extract the value of the elastic modulus of the coating. The obtained value was $E = 15$ GPa. No models were used for extraction of the mechanical properties of the coatings, since it was not possible to obtain a good fit with models proposed in the literature [30–32,38–40]. This may be due to the fact that these models assume that the coating will have the same properties, whereas the studied materials presented particle packing and densification effects due to the SiO_2 nanoparticle reinforcement to the TEOS–MTES coatings.

The adhesive and frictional behaviour of the two types of films was analyzed with the results of the nano-scratch tests, searching for delamination, chipping or plowing events.

Figs. 7 and 8 show the surface profiles of stainless steel plates coated with the bi-layered TEOS–MTES–$SiO_2$10 and 30 wt.%, respectively. The scratch depths (nm) are plotted as a function of both the horizontal displacements (μm) and the normal load applied (mN). The curves illustrate the sample behaviour during the pre-scan,

Table 1
Young's modulus (E) and hardness (H) values found for TEOS–MTES–$SiO_2$10% and 30% coatings on 316L stainless steel (SS) with nanoindentation at deformation rate 0.05 s^{-1}.

	E (GPa)	H (GPa)
AISI 316L substrate (SS)	187 ± 18	2.3 ± 0.1
SS + TEOS–MTES coating	6.5*	0.92*
SS + TEOS–MTES–$SiO_2$10% coating	14 ± 3	1.8 ± 0.3
SS + TEOS–MTES–SiO_2 30% coating	16 ± 3	2.5 ± 0.3

*Values from Ballarre et al. [16].
Substrate and TEOS–MTES coating are shown as reference.

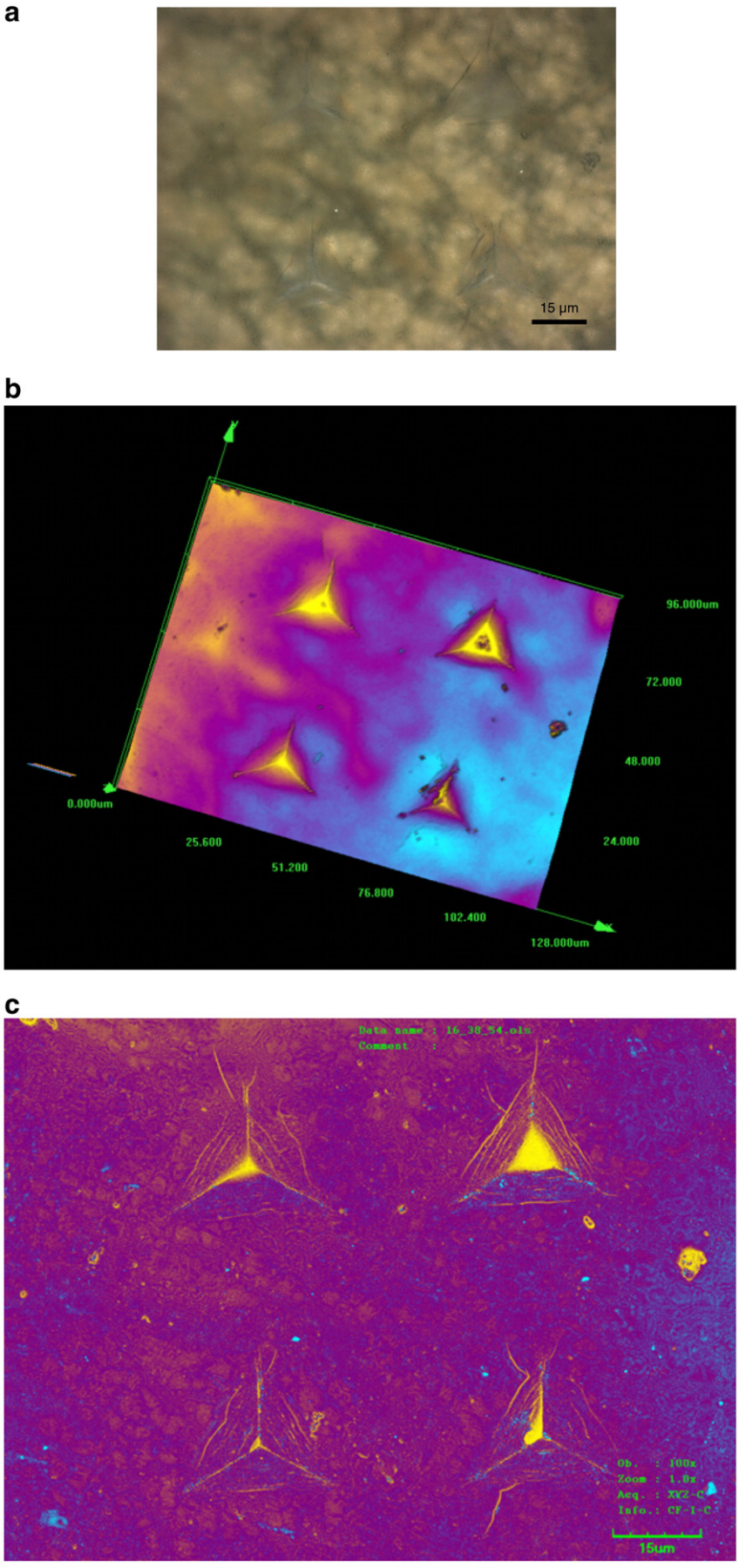

Fig. 6. Confocal Microscope images for the indentation place of the sample coated with TEOS–MTES–30% SiO_2: (a) surface morphology, (b) confocal two dimensional image and (c) confocal three dimensional image.

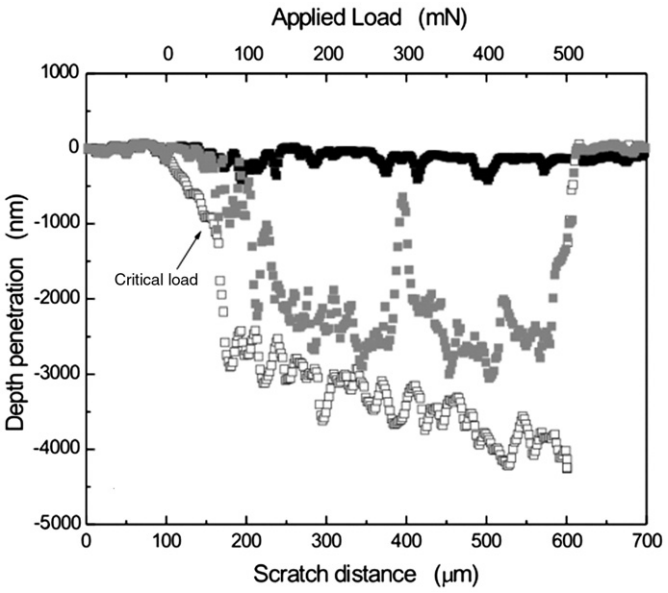

Fig. 7. Scratch depth profile as a function of increasing normal load and as a function of displacement of the indenter tip of the TEOS–MTES–10%SiO_2 film on surgical grade stainless steel. The pre-scan (■), scan (□) and post-scan (■) made is shown.

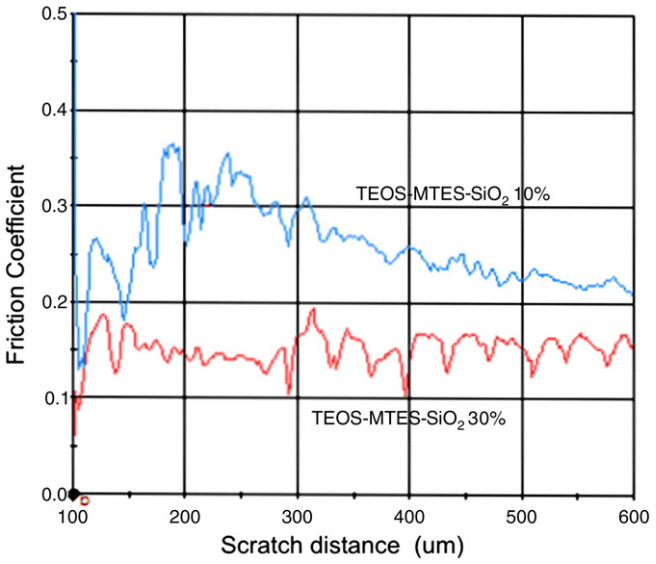

Fig. 9. Coefficient of friction (COF) as a function of increasing scratch distance for the TEOS–MTES coatings reinforced with 10% (-----) and 30% (-----) of SiO_2 nanoparticles on surgical grade stainless steel.

scratching and post-scan test steps. The initial scan at a continuous low load applied is used to analyze the roughness of the film surface through the pre-scan profile obtained. This profile is used in relation to the post-scan in order to evaluate surface damage, debris production and elastic-plastic deformation after the scratching. Negative depths correspond to the scratch indenter being pushed into the film, and positive depths indicate outward blistering of the surface or the accumulation of debris during the scratch test.

Fig. 7 shows the scratch distance versus the applied normal load (or the horizontal displacement) of the TEOS–MTES–$SiO_2$10 wt.% coating. The critical load to produce the failure of the coating is 60 mN, after a total elastic recovery at previous applied loads. This adhesion force and the post-scan curve show clear fracture processes at early times, indicating some delamination events that could lead to fracture and material release to the sides of the indentation trace. The TEOS–MTES–SiO_2 30 wt.% coating scratch test is shown in Fig. 8, in this case the failure takes place at 200mN of applied load, indicating a much better adhesion than the system with 10% of SiO_2 nanoparticles. The peak present in the post-scan around the 250 nm scratch distance position can be attributed to the presence of debris in the trace, showing a slight failure in the coating. This fact could be due to the presence of chipping. Chipping is produced by radial crack formation and subsequent delamination where the area of damage is delimitated by radial cracks [41]. In both cases an elastic recovery is present, due to compact packing of the elastic nanoparticles at low applied loads.

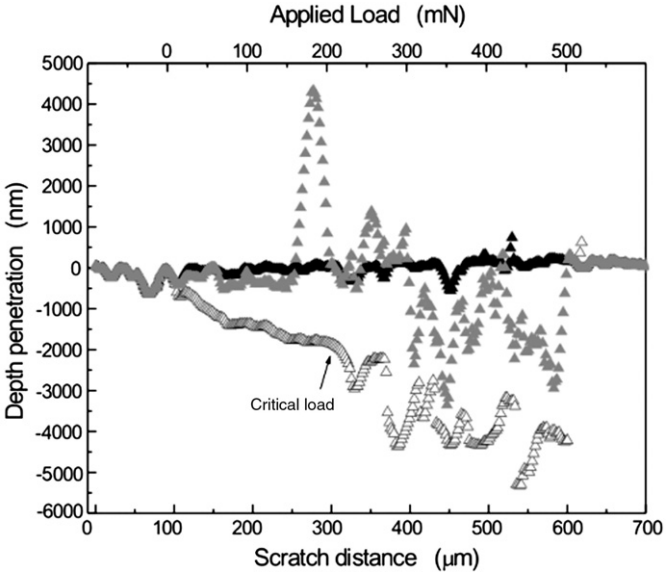

Fig. 8. Scratch depth profile as a function of increasing normal load and as a function of displacement of the indenter tip of the TEOS–MTES–30%SiO_2 film on surgical grade stainless steel. The pre-scan (▲), scan (Δ) and post-scan (▲) made is shown.

The coefficient of friction of the coatings made by TEOS–MTES–SiO_2 with10 and 30 wt.% of silica nanoparticles presented differently notorious values: 0.30 for 10% and 0.16 for 30% of silica nanoparticles present in the inner layer, as can be seen in Fig. 9. The values were taken for the early stages of the friction coefficient vs. scratch displacement curve, when the coating is still unbroken, before the critical load for failure occurs. The COF values also are affected by two contributions: one related to the plowing or abrasion and the other to adhesive component of the forces [33]. The differences in the COF value corresponds to earlier fracture processes in TEOS–MTES–10% SiO_2 coatings and to a better frictional behaviour of the coating with higher amount of silica nanoparticles, making the inner layer more adhesive to the substrate. These values show correspondence with the nano-scratch behaviour explained before.

4. Conclusions

Coatings made by sol–gel method with TEOS, MTES and colloidal silica nanoparticles as precursors were applied on 316 L stainless steel with the aim of providing protective and homogeneous properties to the surface. The addition of silica nanoparticles provides an alternative for the enhancement of film thickness, giving them better elastic-plastic properties. After 1 and 30 days of immersion of the coated system in simulated body fluid, no alterations or significant superficial changes were shown by the SEM examination.

The coatings with the highest amount of silica nanoparticles reinforcement (30 wt.%) presented the best mechanical properties: higher elastic modulus, hardness and failure load in nano-scratch tests. This fact could be due to some compact packing of the elastic SiO_2 particles inside the coating with applying load, acting as a valid

reinforcement, enhancing the ability of these coatings to support the extreme surgical procedures taking place in orthopaedic replacements.

Acknowledgments

The authors would like to thanks the National Research Council of Argentina (CONICET), and National University of Mar del Plata (UNMdP) for the financial support. Also J. Ballarre would like to thanks Dr. F. Sangermano for the great help.

References

[1] J.V. Sloten, L. Labey, R.V. Audekercke, G. Van der Perre, Biomaterials 19 (16) (1998) 1455.
[2] Y. Okazaki, E. Gotoh, T. Manabe, K. Kobayashi, Biomaterials 25 (28) (2004) 5913.
[3] T. Hanawa, S. Hiromoto, K. Asami, Appl. Surf. Sci. 183 (1–2) (2001) 68.
[4] J.J. de Damborenea, N. Pellegri, O. de Sanctis, A. Duran, J. Sol–Gel Sci. Technol. 4 (1995) 239.
[5] P. Galliano, J.J. de Damborenea, M.J. Pascual, A. Duran, J. Sol–Gel Sci. Technol. 13 (1998) 723.
[6] P. Li, K. de Groot, T. Kokubo, J. Sol–Gel Sci. Technol. 7 (1996) 27.
[7] C. Ohtsuki, T. Kokubo, T. Yamamuro, J. Non-Cryst. Solids 143 (1992) 84.
[8] O. Peitl, E. Zanotto, L. Hench, J. Non-Cryst. Solids 292 (2001) 115.
[9] X. Liu, C. Ding, P.K. Chu, Biomaterials 25 (10) (2004) 1755.
[10] T. Kokubo, H. Kim, M. Kawashita, Biomaterials 24 (2003) 2161.
[11] L.E. Amato, D.A. Lopez, P.G. Galliano, S.M. Cere, Mater. Lett. 59 (16) (2005) 2026.
[12] J. Ballarre, J.C. Orellano, C. Bordenave, P. Galliano, S. Ceré, J. Non-Cryst. Solids 304 (5) (2002) 278.
[13] D.A. López, N.C. Rosero Navarro, J. Ballarre, A. Durán, M. Aparicio, S. Ceré, Surf. Coat. Technol. 202 (2008) 2194.
[14] J. Ballarre, S. Pellice, W. Schreiner, S. Ceré, Key Eng. Mater. 396–398 (2009) 311.
[15] J. Ballarre, D.A. López, W.H. Schreiner, A. Durán, S.M. Ceré, Appl. Surf. Sci. 253 (2007) 7260.
[16] J. Ballarre, D.A. López, A.L. Cavalieri, Thin Solid Films 516 (2008) 1082.
[17] R. Prikryl, V. Cech, L. Zajickova, J. Vanek, S. Behzadi, F.R. Jones, Surf. Coat. Technol. 200 (1–4) (2005) 468.
[18] J. Malzbender, G. de With, J.M.J. den Toonder, Thin Solid Films 366 (1–2) (2000) 139.
[19] G. Wei, B. Bhushan, S. Joshua Jacobs, Ultramicroscopy 100 (3–4) (2004) 375.
[20] S. Simunkova, O. Blahova, I. Stepanek, J. Mater. Process. Technol. 133 (1–2) (2003) 189.
[21] L.Y. Huang, J.W. Zhao, K.W. Xu, J. Lu, Diamond Relat. Mater. 11 (7) (2002) 1454.
[22] X. Li, M. Huang, M. Curry, S. Street, M. Weaver, Tribol. Lett. 19 (4) (2005) 273.
[23] W.C. Oliver, G.M. Pharr, J. Mater. Res. 7 (1992) 1564.
[24] I.N. Sneddon, Int. J. Eng. Sci. 3 (1965) 47.
[25] M.F. Doerner, D.S. Gardner, W.D. Nix, J. Mater. Res. 1 (1986) 845.
[26] W.C. Oliver, G.M. Pharr, J. Mater. Res. 19 (1) (2004) 3.
[27] R.B. King, Int. J. Solids Struct. 23 (1987) 1657.
[28] R. Saha, W.D. Nix, Acta Mater. 50 (2002) 23.
[29] S. Bec, A. Tonck, J.L. Loubet, Phila. Mag. 86 (2006) 5347.
[30] B. Jönsson, S. Hogmark, Thin Solid Films 114 (1984) 257.
[31] D. Chicot, J. Lesage, Thin Solid Films 254 (1995) 123.
[32] A.K. Bhattacharya, D.W. Nix, Int. J. Solids Struct. 24 (1988) 1287.
[33] T.W. Scharf, J.A. Barnard, Thin Solid Films 308–309 (1997) 340.
[34] T. Kokubo, H. Kushitani, S. Sakka, T. Kitsugi, T. Yamamuro, J. Biomed. Mater. Res. 24 (1990) 721.
[35] M.F. Montemor, A.M. Cabral, M.L. Zheludkevich, M.G.S. Ferreira, Surf. Coat. Technol. 200 (9) (2006) 2875.
[36] B.N. Lucas, C.T. Rosenmayer, W.C. Oliver, Mater. Res. Soc. Symp. Proc. 505 (1998) 97.
[37] L. Shen, I.Y. Phang, T. Liu, K. Zeng, Polymer 45 (2004) 8221.
[38] A.M. Korsunsky, M.R. McGurk, S.J. Bull, T.F. Page, Surf. Coat. Technol. 99 (1998) 171.
[39] E.S. Puchi-Cabrera, J.A. Berrios, D.G. Teer, Surf. Coat. Technol. 157 (1998) 185.
[40] D. Beegan, T.M. Laugier, Surf. Coat. Technol. 199 (2005) 32.
[41] J. Malzbender, J. den Toonder, A. Balkenende, G. de With, Mater. Sci. Eng. R 36 (2002) 47.